Influence of ocean heat transport on the climate of the Last Glacial Maximum

Robert S. Webb*, David H. Rind†, Scott J. Lehman‡, Richard J. Healy†§ & Daniel Sigman§

* *NOAA-NGDC Paleoclimatology Program, 325 Broadway, Boulder, Colorado 80303, USA*
† *NASA-GISS, 2880 Broadway, New York, New York 10025, USA*
‡ *INSTAAR and Department of Geological Sciences, University of Colorado, Boulder, Colorado 80309, USA*
§ *Woods Hole Oceanographic Institution, Woods Hole, Massachusetts 02543, USA*

A series of climate simulations using an atmospheric general circulation model shows that maintaining ocean heat transport at close to present-day values, but with otherwise glacial boundary conditions, leads to an enhanced cooling, particularly in the tropics. This is in agreement with recent geochemical evidence from fossil corals, ground waters, and ice. Near-modern ocean heat transport may have been sustained in all ocean basins during the Last Glacial Maximum in order to balance the formation and export of Glacial North Atlantic Intermediate Water.

Until recently, most palaeoclimate reconstructions for the Last Glacial Maximum (LGM) indicated an average 8 °C cooling over land and ocean in the middle to high latitudes[1], up to 6 °C cooling over land in the tropics[1–6], and little change in tropical sea surface temperatures (SSTs)[7,8]. Previous global climate modelling experiments[1,9–13] have been unable to produce the large cooling over tropical land areas when using generally accepted glacial boundary conditions and LGM SSTs from CLIMAP[7,8], indicating little or no cooling of the tropical ocean. However, new palaeotemperature estimates from the Sr/Ca ratio in Barbados corals[14] and noble-gas concentrations in fossil ground waters from near sea level in Brazil[15] indicate a 5 °C tropical ocean cooling, and directly challenge the CLIMAP LGM SST reconstruction for the tropics.

Rather than specifying fixed CLIMAP LGM SSTs as a boundary condition in simulations presented here, we have chosen instead to specify the modern grid-by-grid transport of energy through the ocean (after a modest correction for lowered glacial sea level) to simulate LGM SSTs and associated climate conditions. The resulting simulations indicate that incorporating near-modern ocean heat transport (OHT), reduced glacial atmospheric CO_2 levels, large terrestrial ice sheets, together with feedback mechanisms involving atmospheric water vapour, clouds, and Southern Hemisphere sea ice, are sufficient to lower annual-average global surface temperature by 8 °C and tropical SSTs by 5.5 °C.

Ocean heat transport has been estimated previously using the NASA-GISS 8° × 10° atmospheric general circulation model (AGCM)[16] for both modern and CLIMAP SST distributions and associated boundary conditions. These OHTs were generated by diagnosing the grid-by-grid convergence of ocean heat required to maintain a prescribed SST field and integrating the zonal-average convergences from south to north[17,18] (Box 1). We have made similar OHT calculations for a modern climate but with glacial land–sea distributions (sea level 120 m lower and areas occupied by ice sheets at the LGM defined as land; Fig. 1) to ensure that our simulations conserved energy (hereafter, 'near-modern OHTs'). Although reduced relative to modern, the near-modern OHTs in the Atlantic Ocean were consistently greater than OHTs estimated for LGM climate with CLIMAP SSTs[7,8,18] (Fig. 1). Near-modern OHTs in the Pacific Ocean although slightly elevated relative to modern, were not as large as OHTs estimated for LGM climate with CLIMAP SSTs[7,8,18] (Fig. 1). Global ocean heat convergences (OHCs; Fig. 1) associated with the near-modern OHTs, like modern OHCs, are greater than CLIMAP-inferred values at high northern latitudes (primarily an Atlantic basin effect); however, in the subtropics neither the near-modern nor modern OHCs are as large as those inferred for CLIMAP SSTs (primarily a Pacific basin effect; Fig. 1).

Today's pattern of OHT is northward throughout the Atlantic, balancing a southward equator-to-pole transport of ocean heat in the Pacific and Indian oceans. This general pattern is a consequence of both the basin-scale, wind-driven circulation (which does not transport heat poleward of ~45° in any basin) and the large-scale thermohaline or 'conveyor' circulation[19,20]. A primary feature of the latter is the cooling and sinking of saline surface waters in the subpolar North Atlantic to form North Atlantic Deep Water (NADW). Because this water-mass is largely exported to other basins (where it upwells and is re-warmed), a compensatory return flow at or near the surface is required. The continental positions demand that this be achieved around either or both the southern tips of South America and Africa, resulting in a northward transport of heat in both the North and South Atlantic. If the formation and export of NADW were to cease entirely, there would be no demand for inter-basin exchange of water and ocean heat, and a pattern of Atlantic OHT much like that calculated from CLIMAP SSTs would result (Fig. 1). Early geochemical investigations of the abyssal circulation determined that the formation of NADW weakened markedly during the last glaciation[21–23], consistent with the pattern of OHTs inferred from CLIMAP SSTs. However, later investigations have shown clearly that a shallower deep water-mass formed instead (Glacial North Atlantic Intermediate Water)[24–29]. Recent geochemical box-modelling studies[30], and a comparison of modern and LGM distributions of the $^{231}Pa/^{230}Th$ ratio in sediments (ref. 31) indicate that this water-mass was exported to the Southern Ocean at rates comparable to the export of NADW today. As this export would demand an inter-basin exchange of ocean water and heat more like today's than the one inferred from CLIMAP SSTs, we chose to examine the result of maintaining near-modern OHTs under glacial forcing on LGM climate.

Climate model simulations

We have run climate simulations with the NASA-GISS AGCM[16] at 8° × 10° (latitude versus longitude) resolution. We performed a LGM simulation (LGM-A) using these near-modern OHTs, orbital

Box 1 Ocean heat convergence and transport calculations[17]

Ocean heat convergences and associated transports are calculated as the amount of energy advected either into or from each grid box by the ocean that would be required to maintain prescribed SSTs given the energy contribution to each grid box by the atmosphere. Within the GCM, the ocean heat convergence for each grid box is the residual amount of heat necessary to balance the sum of model-provided surface atmospheric energy fluxes:

Ocean heat convergence = net solar radiation + net thermal radiation + latent heat flux + sensible heat flux + precipitation heat flux

Northward ocean heat transports (OHTs) for each ocean basin are calculated as the latitudinally integrated sum of ocean heat convergence for each grid box starting from 90° S and ending at 90° N. The application of modern OHTs in a modern climate experiment will result in predicted SSTs and atmospheric conditions that are nearly identical to the comparable experiment with fixed modern SSTs. Likewise, application of CLIMAP OHTs in an LGM climate experiment will result in predicted SSTs and atmospheric conditions that are nearly identical to the comparable experiment with fixed CLIMAP SSTs.

forcing[32] appropriate for 18,000 yr ago, lowered sea level, LGM terrestrial ice sheets, and modern atmospheric CO_2 levels. A second LGM simulation (LGM-B) was run identical to LGM-A except that a glacial atmospheric CO_2 level of 200 p.p.m. (ref. 33) was specified. Both of these simulations were designed to be directly comparable with a previous NASA-GISS AGCM LGM simulation[11] run using similar glacial boundary conditions, CO_2 set at the glacial level of 200 p.p.m. (LGM-C), and SSTs fixed from CLIMAP[7,8] with implied OHT/OHC as a climate forcing that is very different from modern.

The new palaeoclimate simulations, LGM-A and LGM-B, showed respectively 4.6 °C and 8 °C reductions in global annual-average surface air temperature relative to the modern control simulation (Table 1; Fig. 2). The cooling in both simulations resulted from global increases in planetary albedo, surface albedo, snow cover, ocean ice cover, and both total and low-level clouds, as well as decreases in evaporation over the ocean and in atmospheric water vapour concentrations (Table 1; Fig. 2). Although the reduction of CO_2 in LGM-B contributed only 0.6 °C in direct cooling, the consistently larger feedbacks in this simulation, including a 37% decrease in atmospheric water vapour, resulted in a global cooling almost double that simulated in LGM-A. Based on previous energy-balance diagnostics[11,34], we estimate that the cumulative effects of changes in radiative forcing sum to 5.5 °C cooling in the global annual-average surface air temperature for LGM-A and 8.8 °C cooling for LGM-B (Fig. 3a, Table 1). The dominant radiative cooling was due to reductions in atmospheric water vapour and high clouds which decreased greenhouse forcing, and increases in low clouds which raised the planetary albedo. The small discrepancies between the model simulated temperatures (4.6 and 8 °C) and our estimates for the cumulative effects (5.5 and 8.8 °C) can be attributed to unaccounted for and/or overlapping feedbacks among the various radiative forcing components.

Within the tropics (16° N to 16° S), LGM-A exhibited a 2.7 °C reduction in annual-average surface air temperature and SST relative to the modern control run, whereas LGM-B showed a 5.7 °C reduction in air temperature and 5.5 °C reduction in SST (Table 1). We estimate that tropical cooling due to changes in the vertical distribution and amount of clouds was 2.8 °C in LGM-A and 4.3 °C in LGM-B. The greater cloud-related cooling in LGM-B is primarily an albedo effect driven by a large (7%) increase in low-level clouds compared to a smaller increase (3.4%) in LGM-A (Table 1), an expected result in view of previous analyses of the NASA-GISS AGCM showing that lower SSTs invariably lead to an increase in low clouds[35]. Atmospheric water vapour within the tropics decreased by 23% in LGM-A and 35% in LGM-B, contributing 1.9 °C and 3.8 °C of cooling, respectively. From energy-balance diagnostics for the tropics[11,34], we estimate that the cumulative effects of changes in the radiative forcing sum to 2.5 °C cooling in annual-average surface air temperature for LGM-A and 7.3 °C cooling for LGM-B (Table 1, Fig. 3b). Whereas most feedbacks contribute to tropical cooling, reductions in the atmospheric flux of static energy out of the tropics, and orbitally forced changes in insolation each contributed some warming to the tropics in both LGM-A and LGM-B (Table 1).

Compared to the previous NASA-GISS LGM simulation using fixed SSTs from CLIMAP[7,8] and CO_2 set at glacial levels (LGM-C)[11], LGM-A and B exhibit much greater cooling (Table 1). All of these LGM experiments exhibit significant increases in global planetary albedo primarily associated with large terrestrial ice sheets and expansion of Southern Hemisphere sea ice; however, increases in the planetary albedo in LGM-C were not as large as those in LGM-A and B, reflecting differences in the amount of low-cloud cover and sea-ice cover. The zonal averages of surface air temperature anomalies (Fig. 2) show significantly lower temperatures at all latitudes in LGM-B, whereas the coolings in LGM-A and -C are concentrated in the high latitudes. Evaporation over the ocean in the subtropics is decreased in both LGM-A and B, whereas evaporation is increased or near-modern in LGM-C in response to significantly warmer subtropical SSTs reconstructed by CLIMAP[7,8] (Fig. 2). Within the tropics, zonal-average surface air temperatures in LGM-A and B were 1.1 and 4.1 °C lower, respectively, than in the fixed-SST experiment, LGM-C. Atmospheric water vapour in LGM-A and -B decreased by 22% and 37% globally, respectively, in contrast with only a 12% decrease in experiment LGM-C.

Zonal-average tropical SSTs in the near-modern OHT experiments are 1.4 °C (LGM-A) and 4.2 °C (LGM-B) lower than in the control experiment, in contrast to the 1.2 °C cooling reconstructed by CLIMAP (Table 1). On the other hand, maintaining near-modern OHTs result in LGM SSTs that are 4.1 °C (LGM-A) and 2.9 °C (LGM-B) higher than reconstructed by CLIMAP for the high-latitude North Atlantic (39° to 70° N). However, much of this discrepancy is in the 47° to 55° N latitude band, where SSTs for the different LGM simulations vary between extremes of 6.7 °C and 0.2 °C. Such low temperatures are generally acknowledged to be outside the sensitivity range of SST estimation techniques employed by CLIMAP (that is, $\leq$5 °C)[36]. The annual-average, global sea-ice coverage increased, relative to modern, by 1.6% in LGM-A and 5.5% in LGM-B, whereas, based on the CLIMAP reconstruction, a 4% increase in global sea ice was prescribed in LGM-C. The increase in global sea-ice coverage in LGM-B is dominated by the expansion of Southern Hemisphere sea ice in summer. Comparisons of the zonal-annual averages show LGM-B produced significantly greater Southern Hemisphere sea-ice coverage than reconstructed by CLIMAP, whereas LGM-A produced less (Fig. 2). In the northern North Atlantic, sea-ice cover in LGM-A and in LGM-B was reduced relative to the CLIMAP reconstruction in the central portion of the basin reflecting the greater northern penetration of ocean heat, while approximately the same amount of sea ice was simulated off the coasts of North America and Europe. The locally elevated OHC also resulted in slightly warmer temperatures for North Hemisphere subsurface sea ice between 39° and 70° N, around −4 °C for LGM-A and B versus almost −5 °C in LGM-C with CLIMAP SSTs. The newly simulated sea-ice distributions (LGM-A and -B) are similar to the reconstructed sea surface salinity field for the LGM North Atlantic, showing high salinities (little or no seasonal sea-ice cover) penetrating north to Iceland in the central portion of the basin[37].

The dominant feedback contributing to greater cooling in

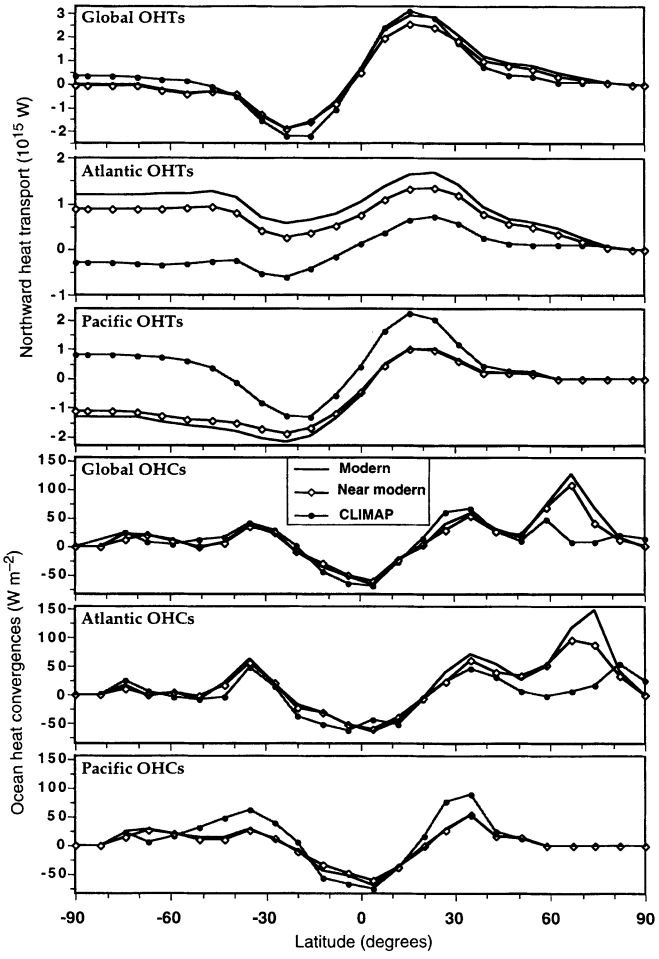

Figure 1 Model-generated annual ocean heat transports (OHTs) and ocean heat convergences (OHCs). Latitudinal zonal averages are shown for the globe, and for the Atlantic and Pacific oceans. The results of three simulations are shown; the modern-climate control experiment (solid black line[4]); the LGM experiment with CLIMAP SSTs (line with filled circles); and the 'near-modern' climate experiment with LGM land-sea distribution (line with open diamonds).

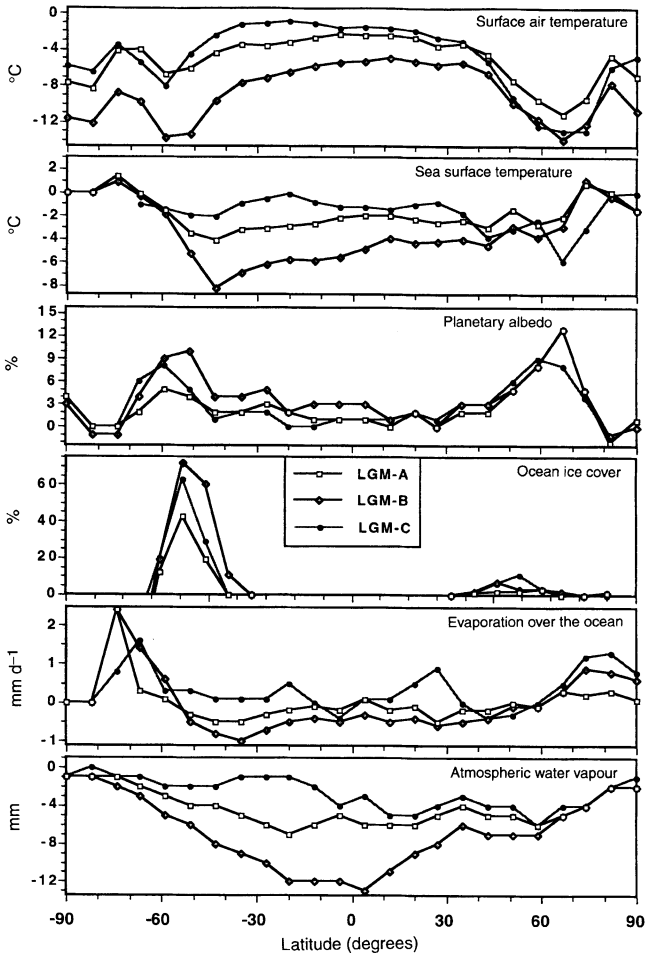

Figure 2 Latitudinal zonal-mean anomalies (experiment minus control) between the modern control climate and the simulated LGM climate: LGM-A (line with open boxes), LGM-B (line with diamonds), and LGM-C (line with filled circles).

LGM-A and B than in LGM-C was changes in evaporation over the Pacific ocean in the subtropics, an area that today is a significant source of heat and water vapour for the atmosphere[38]. Within LGM-C, the sharp gradient of CLIMAP LGM SSTs between the subtropics and the middle-to-high latitudes of the Pacific resulted in high OHCs in the subtropics relative to those associated with modern SST distributions (Fig. 1). Evaporation rates therefore increased in the subtropics in order to balance the increased convergence of ocean heat. The increase in evaporation over the north and south subtropical Pacific in LGM-C was sufficient to compensate for decreases elsewhere, moderating any changes in global atmospheric water content in response to cooler glacial conditions. In contrast, amongst otherwise glacial boundary conditions, the near-modern subtropical OHCs in LGM-A and B result in a decrease in evaporation throughout the subtropics relative to modern, and an even larger decrease relative to LGM-C. The reduction in the subtropics as a source of water vapour for the global atmosphere was amplified in the tropics by a decrease in Hadley circulation in response to lower temperature gradients, which reduced the equatorward flux of water vapour. The combined effects of maintaining near-modern subtropical OHCs (a reduction in OHC relative to CLIMAP), a reduction in atmospheric water vapour, glacial atmospheric CO_2 level, LGM ice sheets, enhanced heat storage in sea ice, and changes in the vertical distribution of clouds are sufficient to have cooled the Earth by 8 °C, and the tropics by 5.5 °C.

In comparison with the 5 °C LGM cooling reconstructed from Barbados corals[14] and noble gases in fossil ground waters from Brazil[15], LGM-B simulated conditions 4.8 °C colder at Barbados and 5.7 °C colder in northeastern Brazil. In contrast, LGM SSTs reconstructed by CLIMAP were less than 2 °C lower than present for Barbados and associated surface air temperatures (experiment LGM-C) were 2.6 °C lower than present for northeastern Brazil. Recent oxygen isotopic measurements in ice cores suggest an 8–12 °C cooling of annual-mean air temperature during the LGM at 6,048 m above sea level in northern central Peru[39]. The simulated cooling at 6,000 m and 8° S was 5.7 °C in LGM-A and 9.3 °C in LGM-B, but only a 2.1 °C cooling was simulated at this location in LGM-C. The annual-average 0 °C isotherm in the tropics dropped by nearly 700 m to ~4,100 m above sea level in LGM-A and by 1,300 m to ~3,500 m above sea level in LGM-B, bracketing the observed LGM snowline depression of 900–1,000 m (ref. 6). In contrast, LGM-C simulated less than a 350-m descent in the 0 °C isotherm in the tropics. The improved match between the palaeoclimate data and the simulated tropical surface air temperatures throughout the lower troposphere of LGM-A, and especially LGM-B, indicate that glacial boundary conditions combined with near-modern OHTs are

Table 1 Global and tropical mean annual anomalies for climate model variables

Variable	LGM-A		LGM-B		LGM-C	
	Global	Tropics	Global	Tropics	Global	Tropics
CO_2 change (p.p.m.)	0.0	0.0	115 (−0.6)	115 (−0.6)	115 (−0.6)	115 (−0.6)
Solar irradiance ($W m^{-2}$)	−0.10	0.75 (0.75)	−0.10	0.75 (0.75)	0.00	0.00 (0.0)
Surface air temperature (°C)	−4.62 (−5.5)	−2.68 (−2.5)	−8.06 (−8.8)	−5.68 (−7.3)	−3.72 (−4.4)	−1.55 (−3.3)
Sea surface temperature (°C)	−1.32	−2.68	−3.49	−5.53	−2.3[7]	−1.25
Ground albedo	4.04 (−1.6)	0.25 (−0.2)	6.15 (−2.4)	0.25 (−0.2)	4.10 (−1.6)	0.00 (0.0)
Land surface albedo	7.29	0.50	7.95	0.50	6.30	0.00
Snow cover (%)	7.00		11.20		8.20	
Ocean ice cover (%)	1.6		5.50		4.10	
Total cloud cover (%)	0.60 (−1.4)	−0.88 (−2.8)	1.30 (−1.8)	−0.38 (−4.3)	0.10 (−0.7)	5.85 (−2.0)
Low cloud cover (%)	2.30	3.40	4.00	7.08	1.50	1.30
High cloud cover (%)	−1.50	−6.08	−2.30	−6.25	−0.90	−3.00
Planetary albedo	2.32	1.75	3.65	3.50	2.10	0.75
Atmospheric water vapour (mm)	−4.90 (−2.5)	−6.00 (−1.9)	−8.60 (−4.0)	−12.25 (−3.8)	−3.00 (−1.5)	−3.50 (−0.6)
Net radiation at the surface ($W m^{-2}$)	−6.5	−6.50	−11.7	−12.75	−5.7	−3.75
Sensible heat flux ($W m^{-2}$)	−1.1	−0.50	−3.1	−2.50	−1.2	0.25
Latent heat flux ($W m^{-2}$)	7.9	2.75	14.8	11.50	3.3	2.50
Static energy flux out of tropics ($10^{14} W m^{-2}$)		12.0 (1.7)		6.0 (0.85)		−1.0 (−0.15)
Precipitation ($mm d^{-1}$)	−0.27	−0.23	−0.51	−0.58	−0.11	−0.05
Soil moisture (mm)	0.00	2.00	3.00	2.25	0.00	2.50

These anomalies are for experiment minus control run. Estimated radiative contributions to temperature change are shown in parentheses. See text for explanation of experiment names.

not only an effective way to cool tropical SSTs, but also permits the model to simulate a reduction in temperature aloft without extreme changes in lapse rates.

OHTs and climate sensitivity

Our results indicate that the new cooler tropical LGM temperatures inferred from coral material and noble gases in fossil ground waters could have resulted from the combined effects of forcing by glacial boundary conditions and of OHTs maintained at near-modern levels during the LGM. In this scenario, high rates of intermediate water formation in the North Atlantic would have been balanced by near-modern transports of ocean heat in the Pacific and Indian basins. Previous climate model simulations have sown that the direct effect of the ice sheets is restricted to a relatively large cooling in northern middle-to-high latitudes[9], whereas modest cooling in low latitudes occurs primarily in response to an overall decrease in atmospheric greenhouse capacity[1,9–13]. In contrast to either the modern climate or our LGM simulations with near-modern OHTs, the previous simulations using CLIMAP LGM SSTs included an implicit increase of OHTs and OHCs as a significant climate forcing mechanism in both the northern and southern subtropical Pacific (Fig. 1) that limits the extent of glacial cooling. Our new simulations indicate that maintaining near-modern OHTs under glacial conditions leads to enhanced global cooling resulting from reductions in evaporation over the subtropical ocean which lead to decreases in global atmospheric water vapour. This cooling mechanism is significantly amplified in response to the effects of reduced levels of CO_2 with greater feedbacks involving atmospheric water vapour, Southern Hemisphere sea-ice growth, and cloud cover changes. The version of the NASA-GISS model used in this study has previously been shown to display enhanced tropical sensitivity related to the explicit representation of cloud generation, penetrative convection and aspects of the hydrological cycle[40]; however, we do not believe that this enhanced tropical sensitivity is the primary explanation for our LGM modelling results. The primary feedback driving enhanced cooling under glacial boundary conditions in these experiments is a change in evaporation controlled by maintaining near-modern OHCs in the subtropical Pacific with high- and low-latitude feedback mechanisms playing less dominant roles. The importance of this feedback mechanism in our simulations highlights the need to re-evaluate CLIMAP LGM SST reconstructions in the Pacific[41], with special attention to the temperature gradient marking the transition between subtropical and subpolar waters.

Our simulations provide a mechanism to cool the tropics by 5–6 °C in accordance with the growing body of new evidence for colder LGM tropical temperatures[14,15,39]. The associated amplified global cooling at the LGM displayed in experiment LGM-B also may have implications for the potential magnitude and distribution of anthropogenic climate change. The simulated 8 °C cooling of global temperature in LGM-B implies a much greater climate sensitivity ($>1\,°C\,W^{-1}\,m^{-2}$) to a total glacial forcing of $7.1\,W\,m^{-2}$ (ref. 42) than previous estimates ($0.5\,°C\,W^{-1}\,m^{-2}$ for a 3.7 °C cooling[11], $0.7\,°C\,W^{-1}\,m^{-2}$ for a 5 °C cooling[42]). Current IPCC assessments[43] conclude that 'the sensitivity of global mean surface air temperature to doubling CO_2 ($4\,W/m^2$ radiative forcing) is unlikely to lie outside the range 1.5 to 4.5 °C', with a best estimate of 2.5 °C (ref. 43), and an implied $0.6\,°C\,W^{-1}\,m^{-2}$ climate sensitivity. Although climate sensitivity may not be symmetric for warming and cooling, from a cold-climate perspective a

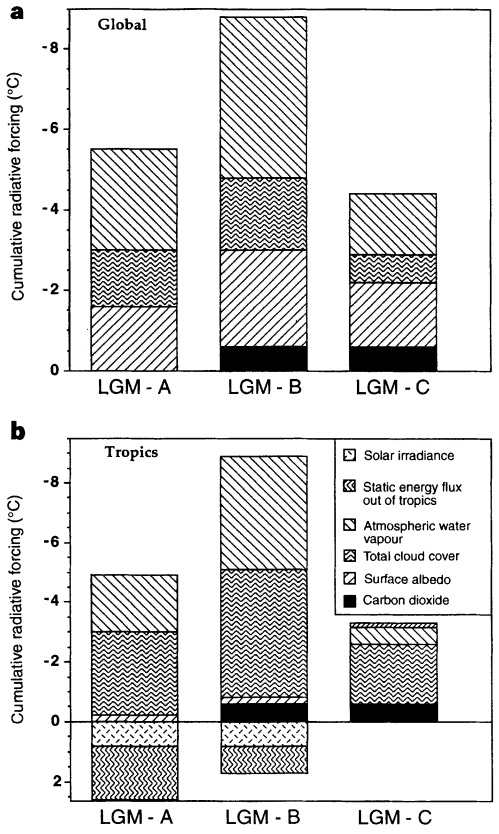

Figure 3 Contributions to the global (**a**) and the tropical (**b**) mean temperature reduction between the modern control climate and simulated LGM climate. Values shown are for the approximate contribution of each component with negative values indicating cooling and positive numbers indicating warming (for example, changes of solar irradiance and static energy flux out of the tropics, as shown in **b**, contribute some warming in LGM-A and B).

$1\,°C\,W^{-1}\,m^{-2}$ climate sensitivity to a $4\,W\,m^{-2}$ radiative forcing may be more appropriate than suggested by IPCC (leading to 4 °C warming), and suggests that inferred climate sensitivity for increased CO_2 under conditions of global warming may be higher than IPCC 'best' estimates[43]. While debate persists on the role and sensitivity of both the tropics and the ocean in future climate change scenarios, our results suggest that under LGM boundary conditions, maintaining near-modern patterns of energy transport from the tropics to high latitudes through the ocean leads to enhanced subtropical and tropical cooling, and cools the Earth. The evidence[6,14,15,39] and possible mechanism for tropical cooling described in this Article undercut arguments that tropical SSTs have changed little throughout the Cenozoic era[44] and that such stability will persist in the future[45]. We recognize that these results could be model-dependent and may reflect how processes are parametrized in the GISS AGCM in comparison to other AGCMs or more complicated coupled ocean–atmosphere–ice sheet models. However, if the coral SSTs and groundwater reconstructions for the LGM temperature are correct, then the $7.1\,W\,m^{-2}$ (ref. 42) glacial forcing requires a climate sensitivity of the order of that shown in our GISS AGCM simulations. □

Received 2 September 1996; accepted 9 January 1997.

1. COHMAP *Science* **241,** 1043–1052 (1988).
2. Colinveaux, P. A. *et al. Clim. Change* **32,** 19–33 (1996).
3. Bush, M. B., Colinveaux, P. A., Wiemann, M. C., Piperno, D. L. & Liu, K. B. *Quat. Res.* **34,** 330–345 (1990).
4. Bonnefille, R., Roeland, J. C. & Guiot, J. *Nature* **346,** 347–349 (1990).
5. Webster, P. J. & Streten, N. A. *Quat. Res.* **10,** 279–309 (1978).
6. Rind, D. & Peteet, D. *Quat. Res.* **24,** 1–22 (1985).
7. CLIMAP Project Members *Science* **191,** 1131–1138 (1976).
8. CLIMAP Project Members *Map Chart Ser.* MC-36 (Geol. Soc. Am., Boulder, 1981).
9. Broccoli, A. J. & Manabe, S. *Clim. Dyn.* **1,** 87–99 (1987).
10. Manabe, S. & Hahn, D. G. *J. Geophys. Res.* **82,** 3889–3911 (1977).
11. Hansen, J. *et al. Climate Processes and Climate Sensitivity* 130–163 (Geophys. Monogr. 29, Am. Geophys. Union, Washington DC, 1984).
12. Manabe, S. & Broccoli, A. J. *J. Atmos. Sci.* **42,** 2643–2651 (1985).
13. Rind, D. *J. Geophys. Res.* **92,** 4241–4281 (1987).
14. Guilderson, T. P., Fairbanks, R. G. & Rubenstone, J. L. *Science* **263,** 663–665 (1994).
15. Stute, M. *et al. Science* **269,** 379–383 (1995).
16. Hansen, J. *et al. Mon. Weath. Rev.* **111,** 609–662 (1983).
17. Miller, J. R., Russell, G. L. & Tsang, L. C. *Dyn. Atmos. Oceans* **7,** 95–109 (1983).
18. Miller, J. R. & Russell, G. L. *Paleoceanography* **4,** 141–155 (1989).
19. Gordon, A. *J. Geophys. Res.* **91,** 5037–5046 (1986).
20. Broecker, W. S. *Oceanography* **4,** 79–89 (1991).
21. Boyle, E. A. & Keigwin, L. D. *Science* **218,** 784–787 (1982).
22. Boyle, E. A. *Annu. Rev. Earth Planet. Sci.* **20,** 245–287 (1992).
23. Curry, W. B. & Lohmann, G. P. *Quat. Res.* **18,** 218–235 (1982).
24. Oppo, D. W. & Fairbanks, R. G. *Earth Planet. Sci. Lett.* **86,** 1–15 (1987).
25. Duplessy, J. C. *et al. Paleoceanography* **3,** 343–360 (1988).
26. Bertram, C. J., Elderfield, H., Shackleton, N. J. & MacDonald, J. A. *Paleoceanography* **10,** 563–578 (1995).
27. Oppo, D. W. & Lehman, S. J. *Science* **259,** 1148–1152 (1993).
28. Boyle, E. A. & Keigwin, L. D. *Nature* **330,** 35–40 (1987).
29. Sarnthein, M. K. *et al. Paleoceanography* **9,** 209–267 (1994).
30. Sigman, D. & Lehman, S. J. *Eos* **46,** F284 (1995).
31. Yu, E.-F., Francois, R. & Bacon, M. P. *Nature* **379,** 689–694 (1996).
32. Berger, A. *J. Atmos. Sci.* **35,** 2362–2367 (1978).
33. Raynaud, D. *et al. Science* **259,** 926–934 (1993).
34. Pollack, J. B. *et al. J. Clim.* **6,** 1719–1742 (1993).
35. Rind, D. *J. Atmos. Sci.* **43,** 3–24 (1986).
36. Imbrie, J. & Kipp, N. G. in *Late Cenozoic Glacial Ages* (ed. Turekian, K. K.) 71–181 (Yale Univ. Press, New Haven, 1971).
37. Duplessy, J.-C. *et al. Oceanol. Acta* **14,** 311–324 (1991).
38. Peixoto, J. P. & Oort, A. H. *Physics of Climate* (Am. Inst. Physics, New York, 1992).
39. Thompson, L. G. *et al. Science* **269,** 46–50 (1995).
40. Rind, D. *J. Atmos. Sci.* **44,** 3235–3268 (1987).
41. Moore, T. C. *et al. Mar. Micropalaeontol.* **5,** 215–247 (1980).
42. Hansen, J., Lacis, A., Ruedy, R., Sato, M. & Wilson, H. *Explor. Res.* **9,** 142–158 (1993).
43. Intergovernmental Panel on Climate Change Working Group I *Climate Change, The Supplemental Report to the IPCC Scientific Assessment* (Cambridge Univ. Press, 1992).
44. Matthews, R. K. & Poore, R. Z. *Geology* **8,** 501–504 (1980).
45. Lindzen, R. A. *Bull. Am. Meteorol. Soc.* **71,** 288–299 (1990).

Acknowledgements. The connection between AGCM results and ocean palaeochemistry grew out of a meeting of the palaeoclimate module of the NOAA-LDEO-SIO Climate Consortium. We thank D. M. Anderson, J. T. Overpeck, M. Chandler, K. Hughen, G. L. Russell, J. R. Miller, W. B. Curry, A. J. Broccoli and M. K. England for discussions and reviews of the manuscript. This work was supported by the NOAA-NGDC Paleoclimatology Program, NASA Climate Program Office, and the US National Science Foundation.

Correspondence should be addressed to R.S.W. (e-mail: rwebb@ngdc.noaa.gov). Model results presented in this Article are available at the World Data Center-A for Paleoclimatology (http://www.ngdc.noaa.gov/paleo/paleo.html).